Waters Symposium

edited by
C. W. Gardner
ChemImage Corporation
Pittsburgh, PA 15208

Evolution of Instrumentation for Detection of the Raman Effect as Driven by Available Technologies and by Developing Applications

Fran Adar*
Raman Spectroscopy Division, 3880 Park Ave, HORIBA Jobin Yvon, Inc., Edison, NJ 08820; **fran.adar@jobinyvon.com*

Michel Delhaye
Technical University of Lille, Lille, France

Edouard DaSilva
Jobin Yvon, SA, 231 Rue de Lille, Villeneuve d'Ascq, France 59650

The evolution of Raman instrumentation from the time of the initial report of the phenomenon in 1928 to the present will be reviewed. The earliest systems were prism spectrographs with photographic plates, and the spectrum was excited with a mercury arc lamp. Because samples were synthesized and then extensively purified to guarantee that the spectrum was representative of the sample, and not impurities, problems of Rayleigh scattering and fluorescence that became important in the period between the 1960s and 1990s were not present. During the period between the mid-1950s to the late-1970s most systems were double grating monochromators, scanned with photomultiplier detectors. During the mid 1970s the first microprobes were introduced on scanning instruments but were then adapted to spectrographs after the multichannel detectors became the method of choice for detection. Initially these were triple spectrographs where the first two stages were used in subtractive mode to filter the laser line, but after the introduction of the holographic notch filters in 1990, a new generation of truly benchtop Raman systems were developed and saw increasing popularity.

General History

The Raman effect was predicted by several physicists between 1923 and 1927 *(1–5)* and first observed in 1928 by C. V. Raman *(6)*. In rapid succession the same effect was observed and reported in several other laboratories worldwide *(7, 8)*. In 1934 Placzek reported a quasi-classical formulation of the effect *(9)*. A time line for the prediction and discovery of the phenomenon and the evolution of the instrumentation is shown in Table 1.

Raman's initial measurements were made on a prism spectrograph, a picture of which is shown in Figure 1. This figure shows a photographic plate on the exit, but, in fact, the earliest measurements were made using the eye as the detector. During the 1930s, 1940s, and 1950s hundreds of compounds were synthesized and studied. Because of the weakness of the Raman effect, samples were purified extensively to maximize the probability that the observed signal could be assigned to the synthesized compound and not to impurities. The equipment used for the observations was based on

Table 1. Timeline for the Prediction and Discovery of the Raman Effect

Year(s)	Event	Year(s)	Event
1922–1927	Theoretical predictions	1971	First instrument with concave gratings introduced by Jobin Yvon
1928	Raman's publication in *Nature*	1972	Characteristics of triple spectrograph described
1934	Placzek's semi-classical theory	1973	Hirschfeld predicted femtoliter sampling
1939	Development of photomultiplier tube	1974	NBS described Microprobe at ICORS; Jobin Yvon exhibited the prototype MOLE
1953	Introduction of Cary 81	1980–1985	Triple spectrographs with multichannel detectors commercialized by Spex, Jobin Yvon, and Dilor
1961	Townes suggested use of HeNe laser as Raman source	1985	Bruce Chase and John Rabolt demonstrated FT–Raman systems with Nd:YAG laser (1064 nm)
1964	Weber, Porto reported first measurement with ruby and HeNe lasers	1990	Carrabba demonstrated holographic filter with small monochromator for acquiring Raman spectrum
1964	Perkin Elmer LR1 with HeNe laser	1991	CCD detectors introduced
1965	Cary 81 converted to accommodate the laser as excitation source; recorded spectrum of 0.25 μL-benzene sample	1992	Renishaw and Dilor introduced first commercially successful benchtop Raman systems
1965	Spex introduced 1401, double monochromator	1993	Stable 785-nm laser source and red-enhanced CCD for near-IR Raman
1966	Delhaye, Migeon proposed microfocusing	1994	Patent for confocal line-scanning issued
1968	First holographic gratings produced	2002	Combination Raman, FT–IR system introduced at Pittcon

Figure 1. Photograph of Raman's spectrograph from the archives of the Indian Association for the Cultivation of Science, Jadavpur, Kolkata; provided by D. Mukherjee.

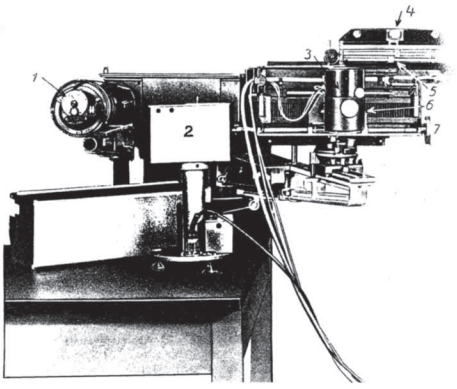

Figure 3. Steinheil Raman spectrometer, shown without the associated electronics, which filled two full-height racks.

large, high-index prisms, and photographic plates. Early workers from Jobin Yvon *(10)* reported using high-aperture lenses to maximize luminosity. The spectra were first generated by filtered sunlight and later mercury arc lamps filtered to pass the excitation line. Because of the long integration times (tens of hours) any particles in the sample would produce flashes of light that would ruin the plates. Therefore the purification process also included filtering. The plates were heated to increase their sensitivity to light, which resulted in the term "baked plates".

Curiously, until the mid 1940s there was much more activity in Raman spectroscopy rather than infrared (IR) absorption because of the relative ease of the Raman measurements over the IR during that period. There were manufacturers of these prism instruments in France (Huet), the United Kingdom (Hilger and Watts), Germany (Steinheil), and Russia (unknown). These instruments were often totally integrated with lamp and detector. After the introduction of photomultiplier tubes (PMTs) in the late 1930s *(11),* these detectors were sometimes offered as an alternative to the photographic plate.

The availability of high-index glass provided good dispersion in the prisms, which could be quite large. Sometimes a large lens was mounted quite close to the photographic plate, which provided a high flux on the photographic plate, all for optimized sensitivity. The dispersion of a prism does not exhibit an analytical function. Its wavelength calibration was achieved by measuring well-known lines of an atomic lamp. Figure 2 shows three spectrographs from Huet and a Raman spectrum superimposed on spectra of the mercury and iron arc lamps. The extraction of frequency shift values from these plates was a tedious process. Figure 3 shows the Steinheill system that utilized three medium-sized prisms (ca. 3–4 cm). This system used both high- and low-pressure mercury arc lamps, and a PMT detector. The slit and PMT were scanned across the focal plane. Collimator and camera mirror focal lengths could be changed to select the dispersion of interest. Figure 4 shows the optical layout of a two-prism spectrograph from Hilger and Watts. This instrument shows both a camera and a PMT. In this system a scanning mirror returned the light from the spectrograph back to the entrance where a slit was mounted. As the angle of the mirror was

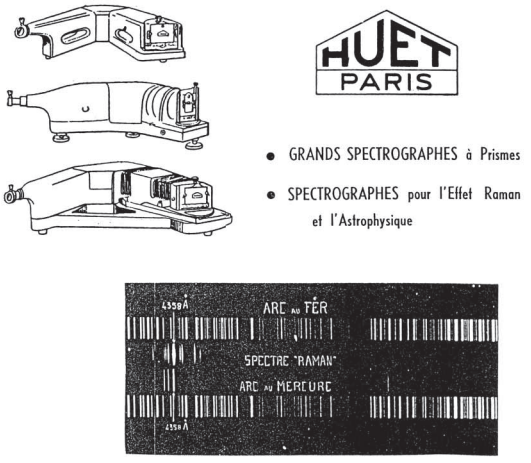

Figure 2. Product literature showing the Huet prism spectrographs, and a photographic plate with spectral lines from the mercury arc, an iron arc, and the Raman spectrum itself.

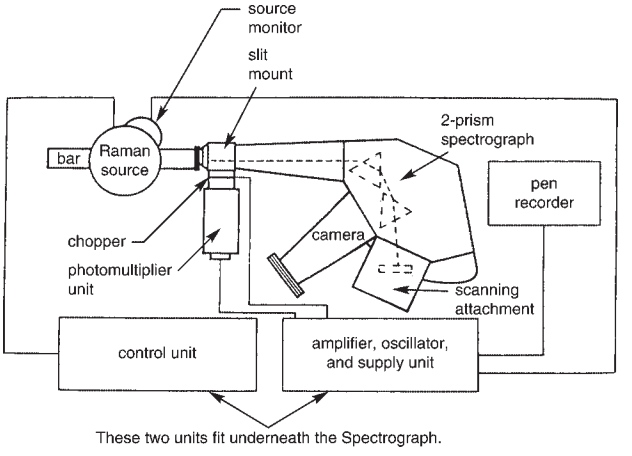

Figure 4. Optical layout of two-prism Hilger and Watts spectrograph, shown with a slit and scanning mirror system to be used with a PMT.

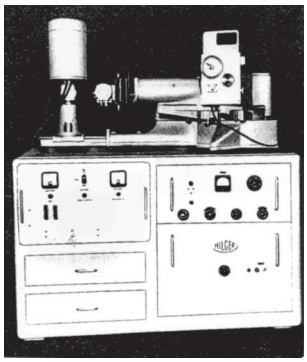

Figure 5. Photograph of full Hilger and Watts system.

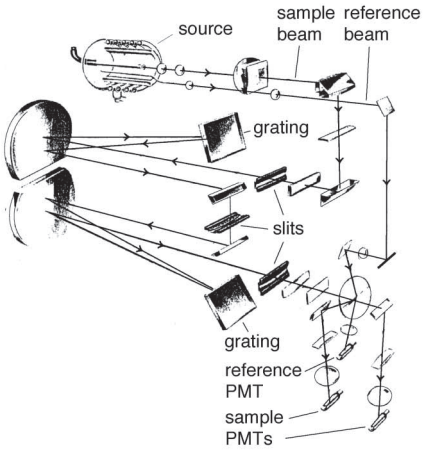

Figure 6. Optical layout of Cary 81, with a Toronto arc lamp.

scanned, the wavelength passing through the slit was changed, and the signal was detected by the PMT. This system was designed in collaboration with Menzies, an advisor to Hilger and Watts. Figure 5 shows the entire system from Hilger and Watts. One can argue that this was an early, fully integrated "table top" system.

The Middle Period: 1950s–1970s

Electronics for single photon counting on PMTs was introduced *(12)*. This meant that, given the optical signal detected, all components of noise were eliminated except for the statistical component inherent in the counting of the photon events itself.

Prism-based instruments were replaced with grating-based instruments, which have the following positive characteristics:

- Good efficiency
- High angular dispersion, with better performance in red
- Analytical description of dispersion, which simplified wavelength calibration
- Large useful area

Double monochromators were built to minimize stray light; their lower efficiency was offset by larger slits that could be used for equivalent resolution. In addition, inteferometric

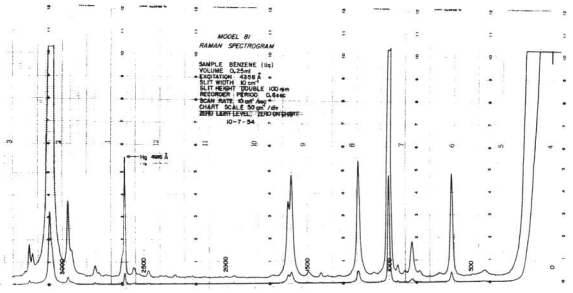

Figure 7. A spectrum of benzene (0.25 μL), ecited at 4358 Å, recorded at 10 cm^{-1} resolution in about 5 minutes with the Toronto arc source.

control was introduced in about 1955 reducing grating ghosts and stray light.

Townes, the inventor of the laser, first suggested the use of the HeNe laser as a Raman source in 1961 *(13)*. The first measurements of Raman spectra excited by the HeNe laser were reported by Weber and Porto *(14)*. As soon as the argon and krypton ion gas lasers were introduced, these lasers were also exploited as Raman sources.

The Cary 81 Raman spectrometer was the first "easy-to-use" system. People reported being able to record spectra as soon as the instruments were delivered to their laboratories. The instrument was introduced at the Molecular Spectroscopy Conference in Ohio in 1954. It used a 3 kW helical Toronto Hg arc, water-cooled for low background, and low pressure for sharp excitation lines. The monochromator was a Czerny–Littrow double, with 1200 g/mm gratings,[1] that was mechanically scanned at speeds between 0.0005 to 50 cm^{-1} s. There were many innovations implemented to optimize its performance:

- Multi-slit design
- Reference phototube
- Plano convex lenses to correct for slit curvature and to reduce aberrations
- The signal was chopped between two PMTs and recombined to recover the lost signal from chopping.
- An image slicer was designed to recover signal lost at the entrance slit when the slit was significantly overfilled by the sample image.

Figure 6 shows the optical layout of the Cary 81 equipped with the Toronto arc, and Figure 7 shows a spectrum representative of its performance. The Cary system was retrofitted with a HeNe laser in 1964 and renamed the Cary 82.

Perkin–Elmer produced the first "benchtop" system in 1966, integrating the laser as a source. It was based on a double-pass monochromator previously used to record infrared spectra. A multipass sample cell was also introduced. Other multistage grating monochromators built during this period are listed in Table 2.

Spectrometer and Spectrograph Design

Grating spectrometers and spectrographs come in several design types. The design is based on several goals. When the signal is detected with a PMT mounted behind an exit

Table 2. Scanning Monochromators with PMTs

Year	Company	Type	Light Source
1953	Cary 91	Double Additive CT	Hg Toronto lamp
1964	Cary 82	Double Additive CT	HeNe laser
1964	Spectra Physics	Double Additive Ebert	HeNe
1964	Steinheil	Double Additive lenses	
1966	Perkin–Elmer	Double Additive CT	
1967	Spex	Double Additive CT	
1967	Coderg	Double Additive CT	
1968	Jarrell Ashe	Double Subtractive CT	
1972	Coderg	Triple Additive SR	
1972	Jobin Yvon	Double Additive concave gratings	

NOTE: CT is Czerny–Turner and SR is Sergent-Rozey.

slit, it is desirable to transfer a tight focus to the slit to maintain optimal spectral resolution. In addition, it is necessary to minimize stray light. The most common spectrometer design is called a Czerny–Turner *(15),* which was created to minimize lowest-order coma, one of the primary optical aberrations. An alternative design to the Czerny–Turner, the Sergent-Rozey *(16, 17),* has been used on several occasions Figure 8 shows the principle governing these two designs. The circle surrounding the grating is the locus of points that minimizes aberrations. For a grating mounted with its grooves vertical, as shown in the figure, slits can be placed along a line transecting the grating either in the horizontal plane or the vertical plane. The tilt of the concave mirrors is then adjusted to correctly send the light through the system. A Czerny–Turner monochromator uses slits along the horizontal trace, whereas the Sergent-Rozey uses the slits along the vertical line.

The Sergent-Rozey system has two advantages that are not well recognized. In the first place spectral anomalies due to re-diffracted light are totally eliminated. The figure shows the artificial spectra in the two designs. In the Czerny–Turner design parts of the spectrum focused by the camera mirror on the slit plane can potentially fall on the grating to be re-diffracted somewhere through the system causing artifacts in the spectrum. In the Sergent-Rozey design the final spectrum is focused *below* the grating where it would not be re-diffracted.

The second characteristic becomes important when designing multistage systems. A double Sergent-Rozey monochromator can be made by mounting the two gratings side-by-side on a single shaft. In that case, no additional mirrors are required to direct the light from one monochromator to the next. This is illustrated in Figure 9 that shows the layout of the T800, which was actually a triple spectrometer. However, the disadvantage of this design was that it takes up more volume. Further modifications were made to the Czerny–Turner design to optimize it for use with multichannel detectors. Ray tracing indicated that asymmetrization would sharpen the slit image *(18),* and flatten the focal surface *(19).*

In 1966, the first holographic gratings were produced using photoresist that was exposed to interfering laser beams. Holographically recorded gratings have the advantage that they eliminate essentially 100% of the ghosts and stray light artifacts of conventionally ruled gratings. Figure 10 shows laser reflection patterns from two gratings of the same groove

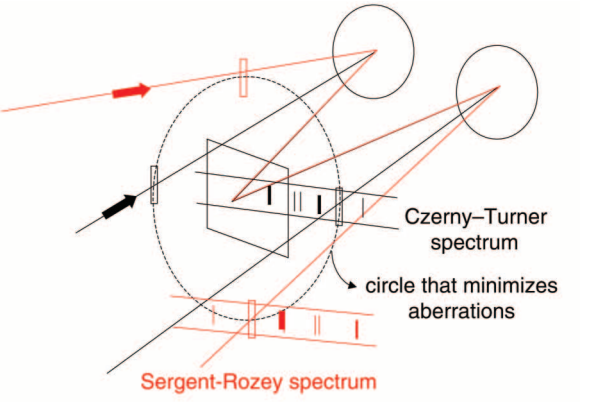

Figure 8. Principle of Czerny–Turner vs Sergent-Rozey spectrometer design. The Czerny–Turner plane is horizontal in this figure while the Sergent-Rozey is vertical.

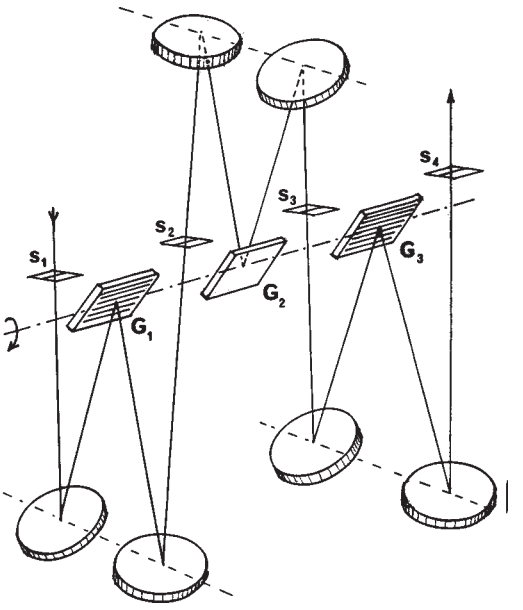

Figure 9. Optical layout of T800, a triple scanning spectrometer of the Sergent-Rozey design: s = slit and G = grating.

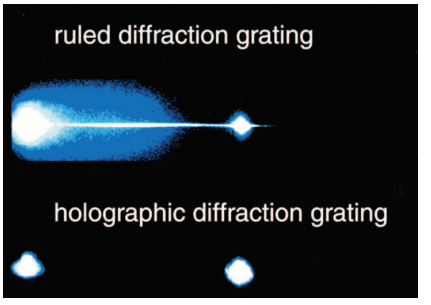

Figure 10. Laser diffraction patterns from conventionally ruled and holographic gratings.

density. The bright spots are diffraction orders. Between and around the diffraction spots from the conventionally ruled grating is a significant quantity of light due to imperfections in the grating. The improvement in performance of holographic gratings has the potential for much improved stray light rejection in Raman spectrometers and spectrographs.

Figure 11 shows the optical layout of the HG2S, the first Raman spectrometer based on holographically recorded gratings. This instrument was introduced in 1971. It was neither a Czerny–Turner nor a Sergent-Rozey. It used concave gratings. It was not necessary to have any optics other than the gratings between the slits. Consequently there were no additional sources of stray light. The low frequency performance of this instrument was significantly improved over anything that preceded it. Spectra could be recorded to frequency shifts lower than 10 cm^{-1}. Figure 12 shows the very low frequency spectrum of SiO_2.

Before the use of computers, spectra were scanned synchronously with strip chart recorders. Most spectrometers have drive systems where linear movement of a stepper motor is related to the wavelength diffracted by the grating. However, the Raman spectrum is described naturally in terms of shifts in the reciprocal of the wavelengths. That meant that a different drive system evolved for Raman instruments. The diffraction equation relating the incident and scattered angles i and i', to the wavelength of light is

$$\sin i + \sin i' = kn\lambda$$

where k is the diffraction order and n is the index of refraction (= 1 in air). Simple geometric arguments indicate how it is possible to devise a mechanical system that can scan in cm^{-1} rather than nm. This is illustrated in Figure 13. The gray-shaded triangles represent the triangles that get pushed by linear motion from a motor and that motion is related in a linear fashion to either the sine or cosecant of the included angle.

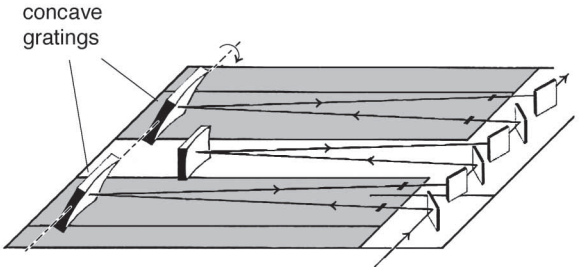

Figure 11. Optical layout of HG2S based on concave holographic gratings.

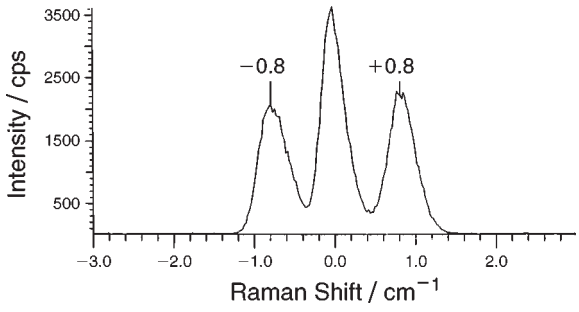

Figure 12. Brillouin spectrum of SiO_2 showing bands at ±0.8 cm^{-1}.

Multichannel Detectors

The development of reliable multichannel detectors in the early 1980s meant that Raman spectra could again be collected in the same "multiplexed" fashion as had been used with the photographic plate, but now with all of the advantages of an electronic detector in terms of signal-to-noise, wavelength response, dynamic range, and digital storage and manipulation. The earliest detectors were the intensified photodiode array and the imaging PMT. The imaging PMT had good noise characteristics but limited dynamic range. The photodiode array was the detector of choice for commercial instruments for years until the maturation of the high sensitivity of the CCD camera. It inherently provided lower noise, and the wavelength sensitivity was not limited to the photocathode of the image intensifier. In addition, it was two-dimensional with the important implication that Raman mapping and imaging had new possibilities.

With the introduction of these detectors, it became clear that the Raman spectrograph needed a total new design to better match the detector size. A typical device had 1000 25 μm pixels, but the coverage on the detector from a double monochromator (which only provided a 18-mm unvignetted field) was about 150 cm^{-1} when the 1800 g/mm gratings were used with an argon laser. In addition, the low frequency performance was significantly degraded when an exit slit with PMT was replaced by larger intermediate slits and a multichannel detector in the focal plane.

The instruments designed specifically to be used with multichannel detectors first included a double subtractive premonochromator to filter the laser beam *(20)*. The focal length and grating groove density of the dispersive stage were selected so that the final coverage was about 1000 cm^{-1}, or 1 pixel/cm. The stray light properties of this design were analyzed carefully in the Ph.D. thesis of Michel Leclercq at the University of Lille *(21, 22)*. Several commercial products have been produced since 1979 and are shown in Table 3. When calibrating spectra on a multichannel array, in principle the wavenumber shift at every pixel can be predicted from the focal length, groove density, and pixel size, once the central

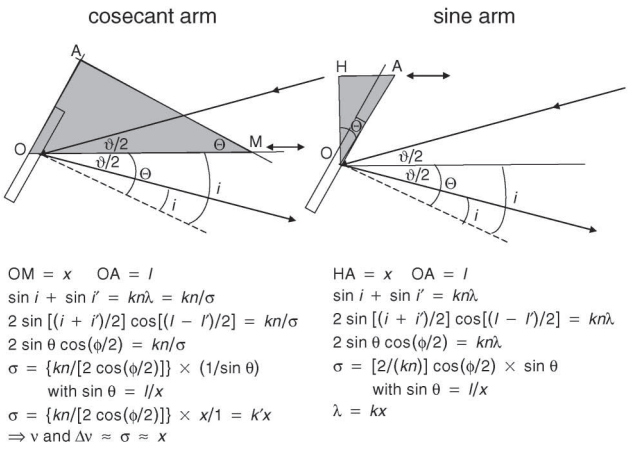

Figure 13. Trigometric description of the cosecant and sine drives—x represents the linear motion of the motor which is converted to angular motion of the grating in units linear with the sine or cosecant of the angle.

Table 3. Commercial Raman Instruments with Multichannel Detectors

Commercial Product	Year of Introduction	Description	Configuration
OMARS89	1979	Multichannel and single channel	(0.5 m)^2(0.4 m/0.3 m)
1877	1981	8-mm intermediate slit, limited coverage	(0.34 m)^2(0.5 m)
MICRODIL28	1981	Confocal laser scanning microscope, (lenses in 3rd stage), patented lens-scanning system	(0.5 m)^3
S3000	1985	—	(0.32 m)^2(0.64 m)
XY	1986	Modular, additive mode, SAS*, csc drive	(0.5 m)^3 or (0.8 m)^3
Jasco	~1987	—	(0.64 m)^2(0.64 m)
T64000	1988	Additive mode, SAS, sine drive	(0.64 m)^2(0.64 m)
Acton	2000	Modular	—

NOTE: SAS means that Stokes and anti-Stokes measurements can be made simultaneously.

pixel is known. Figure 14 illustrates the calculations used to generate this information *(23)*. It is important to realize that the choices in spectrograph focal length, groove density, and pixel size that will be used with a given laser wavelength will determine not only spectral coverage but also resolution, and that resolution cannot be improved beyond the equivalent dispersion in two pixels on the CCD. This resolution will only be achieved with the entrance slit is set to a value between one and two pixels wide. However, on these systems the resolution and coverage can be optimized for a particular measurement by selecting a grating from a number of choices.

Figure 15 shows single shot spectra recorded from polycrystalline graphite using two different gratings (1800 g/mm vs 600 g/mm) and two different laser wavelengths (632.817 and 514.532 nm). The focal length of the system used for these measurements (LabRAM) was 300 mm. The differences in dispersion and coverage are clear. Note that the number of cm^{-1}/Å in the green are about 4 but about 6 in the red. Since the dispersion in Å of a spectrograph is relatively constant, the resolution differences noted between the spectra acquired with the two lasers using a given grating is due principally to the number of cm^{-1}/Å at the two laser wavelengths.

Triple Spectrographs

The principle of a classical triple spectrograph (double subtractive + spectrograph) is illustrated in Figure 16A. The premonochromator presents non-dispersed, but laser-filtered light to the spectrograph stage whose dispersion defines the resolution of the final spectrum. Figure 16B illustrates how this was implemented on the T64000. This instrument has an optical option that can convert the subtractive premonochromator into an additive one. In this case, one can record spectra in both additive and subtractive modes—in one case for high resolution and in the other for high stray light rejection. The spectra reproduced in Figure 17 were recorded from a semiconductor superlattice. Bands down to 4 cm^{-1} are clearly visible. These very low frequency bands have been recorded with a CCD using the system in subtractive mode and with a PMT in additive mode.

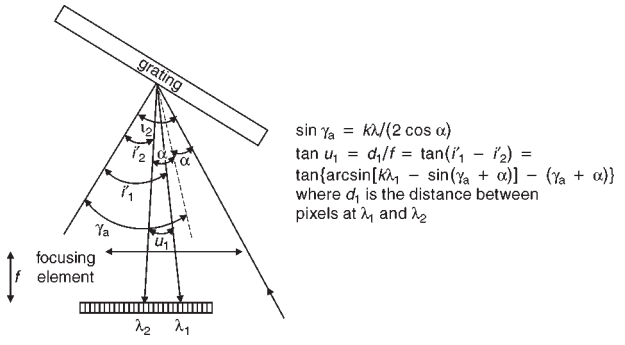

Figure 14. Raman shift calculation for a multichannel detector.

Raman Microscopy

The Raman community initially exhibited very little interest in Raman microscopy. It was argued that because the Raman signal scales with the number of exciting molecules, reducing the sample size would produce unacceptably weak signals. In 1966, Delhaye and Migeon published calculations

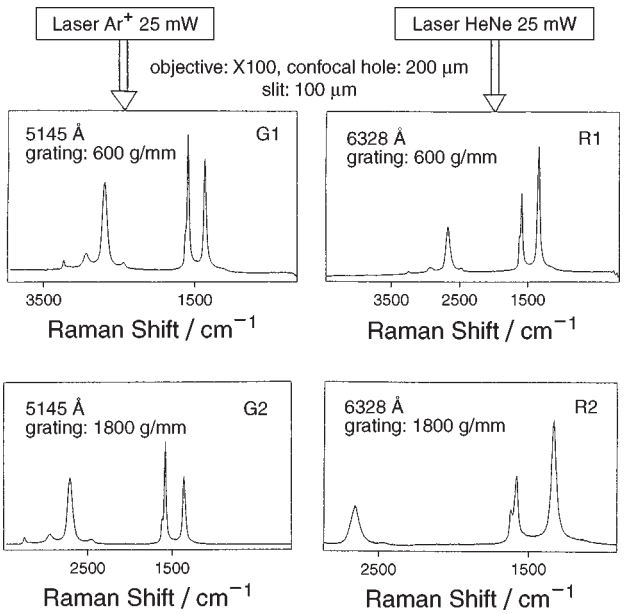

Figure 15. Raman microprobe spectra of polycrystalline graphite recorded on the LabRAM using laser lines at 514.532 and 632.817 nm and gratings with 600 and 1800 g/mm groove density.

(24, 25) that showed that the loss of signal would be fully compensated by the advantages of a microprobe, which include

- Tight laser focus at sample (resolution ~1 μm)
- Raman collection efficiency
- Effective coupling of the sample volume on a small entrance slit.

[According to Delhaye the only Raman researcher who showed an interest was Tomas Hirschfeld, but because of his involvement with the military, little of his work had been published with one exception *(26).*]

It was only in 1973 when Raman microscopy was proven simultaneously in two locations. Paul Dhamelincourt, then a student of Delhaye, assembled a system that proved that a Raman microscope really was feasible. The initial experiments in Delhaye's laboratory showed that it was possible to record a picture of a sample through its Raman light. Subsequently spectra of microparticles were measured. Simultaneously Greg Rosasco and Edgar Etz at the National Bureau of Standards assembled a microprobe based on an elliptical reflector in order to study environmental microparticles. The first publications documenting these experiments appeared in the abstracts for the Raman spectroscopy conference in 1974 *(27, 28).*

Delhaye and Dhamelincourt *(29)* described their imaging Raman concepts in a publication in 1975 where they showed several possibilities for creating a Raman image. These possibilities are illustrated in Figure 18. Based on these concepts the first commercial instrument, the MOLE, was introduced in 1974. The prototype is shown in Figure 19.

This instrument had three modes of operation. It was based on a double monochromator using 1 m concave holographic gratings. When used as a microprobe, a 1-μm laser spot was imaged onto the entrance slit and then onto a PMT. When used as a spectrograph, a SIT or SEC camera was mounted at the exit focal plane and a range of about 100 cm^{-1} could be viewed for kinetic measurements. When used as a Raman microscope, the sample was illuminated globally and it was imaged onto the grating rather than the slit. The image of the sample, after being diffracted by the grating, was projected onto the camera. Figure 20 shows the results of these three modes of operation on a mixture of MoO_3 and K_2CrO_4.

Raman Microprobe

The success of a Raman microprobe is based on four optical properties:

- Laser focal spot at the sample
- Collection efficiency of the microscope optics
- Efficiency of the coupling of the light coming from the laser focal volume and the spectrometer or spectrograph
- Confocal principle

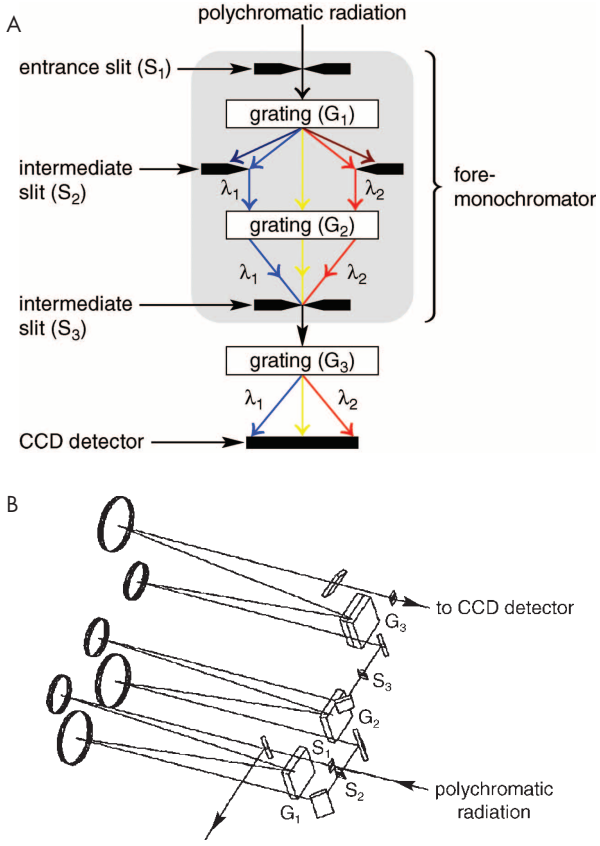

Figure 16. (A) Principle of triple Raman spectrograph with double subtractive foremonochromator. (B) Optical layout of T64000 in subtractive mode. Because of the reversal of the sense of dispersion of gratings G_1 and G_2, the slit S_3 sees nondispersed light that has been filtered by the foremonochromator. The coverage is determined by the size of the slit S_2, which can be as large as 50 mm.

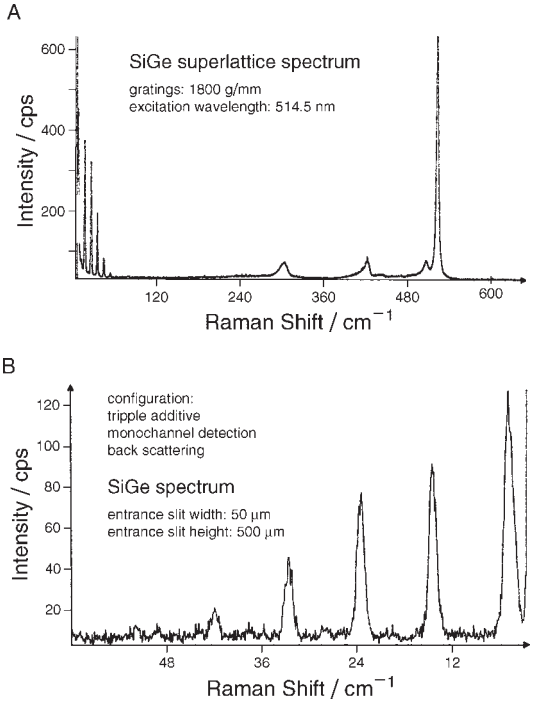

Figure 17. (A) SiGe superlattice spectrum recorded on T64000 working in subtractive mode with a CCD detector. (B) SiGe superlattice spectrum recorded on T64000 working in additive mode with PMT. Note that the ultimate low frequency performance is achieved in this mode of operation.

The Raman microprobe is based on the recognition of the focusing properties of high numerical aperture (NA) objectives. The beam spot size w, of a laser beam entering a well-corrected objective is

$$\omega \approx \frac{\lambda}{NA}$$

This equation indicates that the spot size decreases as the wavelength of the radiation decreases and as the NA increases. For visible radiation and 100× objectives (NA > 0.9), it is easy to achieve spot sizes under 1 μm.

The collection efficiency is also determined by the NA of the objective. Good, high NA microscope optics far exceed even the best macro Raman sampling optics. Figure 21 shows the results of calculations illustrating this point. Figure 22 shows the principles of the scheme to transfer the Raman light collected by the objective to the entrance slit. Not only is the laser focal volume at the sample imaged on the entrance slit (and later on the detector), but the back aperture of the objective is imaged onto the grating, the limiting aperture of the spectrograph. For this reason multiple lenses are used in the optical train. The top of the figure illustrates this principle; the bottom part of the figure illustrates its implementation. Note that between the microscope and the spectrograph there is an intermediate image plane at which is mounted a hole that is "confocal" to the sample and the entrance slit. The principles for this coupling was described in a publication by Dhamelincourt *(30).*

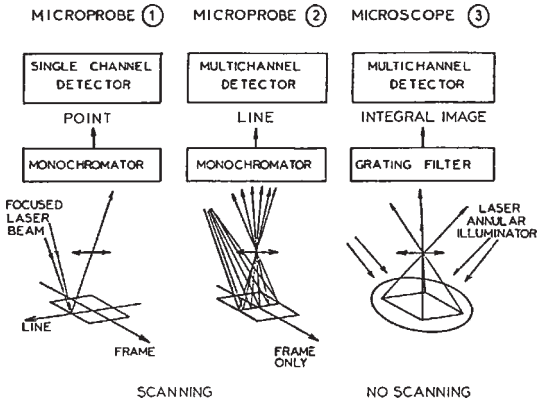

Figure 18. Various schemes for Raman imaging. (Reproduced with permission: Delhaye, M.; Dhamelincourt, P. *J. Raman Spectrosc.* 1975.)

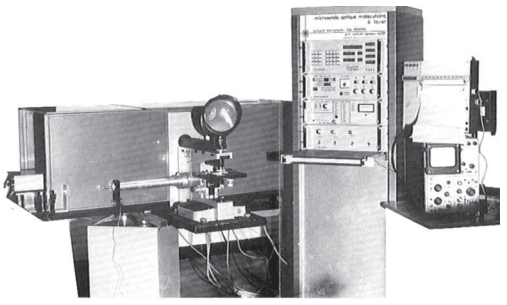

Figure 19. Prototype MOLE Raman microscope.

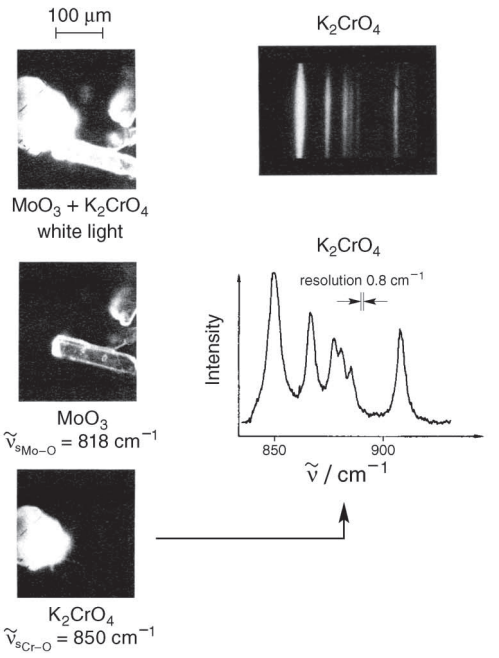

Figure 20. Three modes of operation of MOLE. Upper left shows a white light image. The two lower left images show Raman micrographs in lines of MoO_3 and K_2CrO_4. Upper right shows the spectrum of the chromate species on the multichannel detector and the lower right shows the PMT output of the same spectrum.

	OPTIC	NA = $n\sin\theta$				
		n = 1	n = 1.33	n = 1.5	θ	Ω/2π
	f/10	0.0499	0.066	0.74	2.862	0.06
	f/5	0.099	0.131	0.148	5.71	0.25
	f/4	0.124	0.165	0.186	7.125	0.38
	f/3	0.164	0.218	0.246	9.462	0.68
10x	*f*/1.93	0.25	0.332	0.375	14.477	1.5
M Chamber	*f*/1.8	0.267	0.355	0.4	15.485	1.8
M Chamber2	*f*/1.4	0.336	0.447	0.504	19.633	2.9
20x ULWD	*f*/1.14	0.4	0.532	0.6	23.578	4.1
	f/1	0.44	0.594	0.67	26.551	5.2
50xULWD	*f*/0.75	0.554	0.737	0.831	33.69	8.4
50x	*f*/0.44	0.75	0.997	1.125	48.59	16.9
100x	*f*/0.164	0.95	1.263	1.425	71.8	34.3

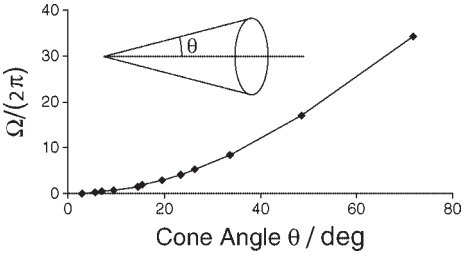

Figure 21. Top: Tabulation of relationship between *f*/#; NA; collection efficiency, Ω/2π; and θ, the included half angle of the optic. Bottom: Definition of optical angle θ and collection efficiency, Ω/2π. Note that *f*/1 corresponds to 26°, but its collection efficiency is about 1/4 that of a 100× microscope objective.

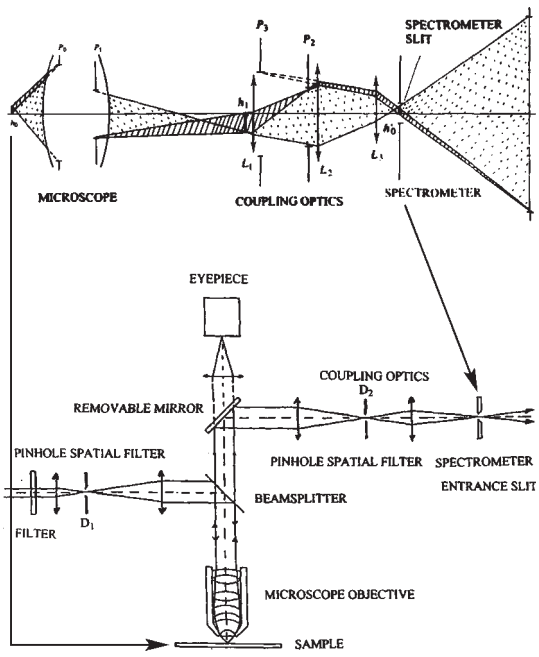

Figure 22. (Top) Optical principle describing how light is collected and imaged from the Raman volume to the spectrograph. (Bottom) Implementation of this principle. Note the pinhole spatial filter that will serve as a confocal hole for increased spatial resolution. These figures are reproduced from Figures 9 and 10 of ref *31*.

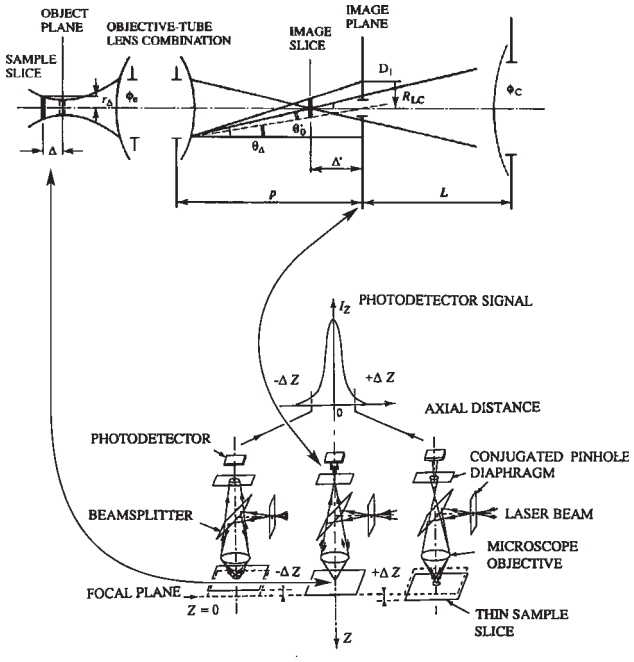

Figure 23. Principle of confocality: only light being emitted from the focal plane of the instrument will be efficiently transmitted by the confocal aperture and onto the detector. These figures are reproduced from Figures 11 and 13 of ref *31*.

The principle of confocality is described in Figure 23. The idea is that insertion of an aperture in a plane conjugated to the plane of analysis will block Raman radiation emitted by material surrounding the laser-irradiated volume. This has the effect of assuring that the Raman spectrum represents the material of interest, as well as blocking fluorescence and Rayleigh light. The degree of confocality will be determined by the size of this hole relative to the size of the image, as well as the NA of the microscope optics.

The early 1990s saw the development of a method to map samples confocally while multiplexing the laser beam on the sample and taking advantage of the second dimension of the CCD *(32)*. The principle is shown in Figure 24. The laser is scanned across the back aperture of the objective in such a way as to avoid introducing aberrations and then losing the diffraction limit in the laser spot. The Raman light returns on the same scanning mirror so that it can be then focused through the confocal hole and rescanned onto the entrance slit of the spectrograph. Each point on the slit represents Raman signal from a confocally defined spot on the sample. By appropriately processing the signal on the CCD, one can construct a Raman map that is truly confocal.

While certainly Raman micrographs can be recorded directly as was shown earlier, the confocal mapping provides significant advantages to these capabilities. Raman signals tend to be weak and are easily overwhelmed by background signals. In the case of microscopy, this can be matrix signals (i.e., from material around the directly illuminated spot) as well as luminescence and Rayleigh light. Confocal aperturing reduces most of these unwanted signals so that the resulting Raman images have much better contrast. While sometimes it is possible to subtract these background levels, subtraction will never remove the noise created by high background levels. Figure 25 shows the results of a confocal map of a histological section containing Dacron (polyethylene terephthalate) fibers with adhering protein. Note that this map was performed with a HeNe laser on a "real-world" sample.

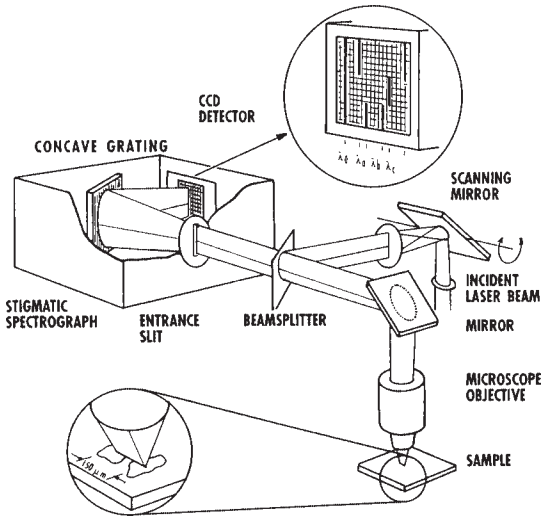

Figure 24. Optical scheme for confocal line-scanning. Reproduced from Figure 7 of ref *38*.

The Current Period

Several technologies have been important for the rapid increase in Raman use over the past decade. They include

- Multichannel detectors
- Air-cooled lasers
- Desktop computers
- Holographic notch filters

The one item on this list that is most specific to Raman instrumentation is the holographic notch filter. Carrabba *(33)* made the first measurements with this class of filter and showed that it would no longer be necessary to use large instruments for many routine Raman measurements. The physical principles of volume holography were laid out in 1993 *(34)* and will certainly be covered in detail in Harry Owen's contribution.

However, there is an historical curiosity that has come to our attention. In a 1948 publication in France, J.-L. Delcroix reported the use of "Lippman plates" as filters *(35).* Gabriel Jonas Lippman had received the Nobel Prize in 1908 for "for his method of reproducing colors photographically based on the phenomenon of interference". The Lippmann reflection filters were based on gelatin, with silver films on them, and a mercury layer assuring reflection. Delcroix notes that these filters can reflect a particular wavelength (which will depend on the angle of incidence) but transmit all others. To quote him "En particular, Mr. Kastler avait en l'idee d'utiliser les plaques Lippmann, dans l'obtention des specters Raman, pour affaiblir la raie excitatrice si genante dans l'etude des raies de basses frequencies." (In particular, Mr. Kastler had the idea to use the Lippmann plates in order to obtain Raman spectra, by reducing the exciting ray that is troublesome in the low frequency region.)

Benchtop Instruments

Following the recognition that the notch filter could enable the construction of Raman instruments of vastly reduced size, benchtop instruments appeared on the market. Because of their reduced complexity, much less light was lost in the optics and much more reached the detector. The CCD, a multichannel detector with extremely low noise became the detector of choice. Spectra could now be recorded in seconds to minutes instead of hours. Highly powerful desktop computers made instrument control and data treatment very sophisticated. Systems really can be turn-key and easy-to-use.

The availability of long wavelength red lasers (785 or 830 nm) provides almost fluorescence-free results for "dirty" organic materials. UV optics are now available for UV Raman microscopy, and its application is certain to have an impact in semiconductor studies. However, application of these systems is sometimes limited by laser-induced photochemistry, especially of organic materials so the universal usefulness may not be achieved.

Near-field micro-spectroscopy *(36)* is certainly a field that is showing some interest, but whether there is sensitivity for a true near-field Raman signal is in controversy. Conversations both with Aaron Lewis of Nanonics and Bruce Chase of DuPont have indicated that the sensitivity is not adequate. What can be useful, however, is the ability to identify a good region for analysis and then to do the Raman microanalysis in the far field.

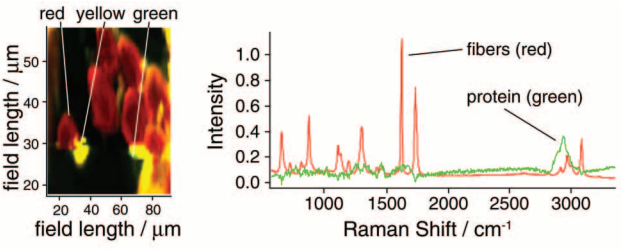

Figure 25. Confocal map of Dacron fibers in histological section: proteins appear green, fibers appear red, and the proteins that overlay the fibers appears yellow. A color version of this image is located in the table of contents.

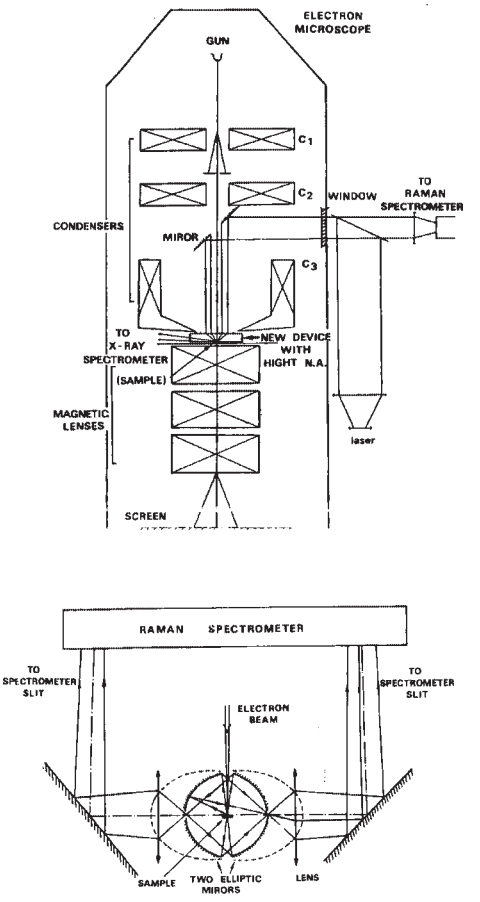

Figure 26. Schematic of proposed implementation of a Raman microprobe in an electron microscope. Figures from ref *37,* p 164.

Another area that has shown some interest is the integration of a Raman probe with an electron microscope (Figure 26). This is interesting because Delhaye's original interest in the Raman microprobe was generated by his interaction with Castaing and the developing electron microprobe of the time. Delhaye has proposed that elliptical reflectors could be introduced in an electron microscope at the sampling point and coupled to a laser and Raman spectrometer *(37).*

Closing Remarks

Certainly when reviewing the evolution of Raman instrumentation, one is struck by the cycling of many concepts. The first instruments were prism-based spectrographs using lenses for collimation and focusing. Today's instruments are also spectrographs, but they use CCD cameras instead of photographic plates. While mirror-based spectrometers were used almost exclusively in the middle period, benchtop instruments working in the visible today use lenses with their superior focusing properties. There is of course no analog to the laser source in the earlier instruments. But the real surprise in researching this article was the discovery that the Lippmann filter technology, which appears to be a pre-laser replica of today's holographic filters, was suggested as a means to suppress the source scattering in a Raman spectrum. The major difference, that the holographic filters are produced with lasers, affords superior control of the production of the filters.

The take-home message is that many of the ideas that make the current instruments so successful were tried at various times over the previous 80 years. But all these technologies converge today to produce the quality of instrumentation that has shown such promise for the future of materials analysis.

Acknowledgments

The authors wish to thank the following for helpful discussions in preparation of this manuscript: Michael Carrabba, Paul Dhamelincourt, John Ferrarro, Michel Leclercq, Joel Oswalt, Anant Ramdas (Raman's last student), Hans Juergen Reich, Bernard Roussel, Steve Slutter, Alfons Weber, and Andrew Whitley.

Note

1. Grooves per millimeter is expressed as g/mm.

Literature Cited

1. Raman, C. V. *Proc. R. Soc. London, Ser. A* **1922,** *101,* 64.
2. Smekal, A. *Naturwissenschaften* **1923,** *11,* 873.
3. Kramers, H. A.; Heisenberg, W. *Z. Phys.* **1925,** *31,* 681.
4. Schroedinger, E. *Ann. Phys*. **1926,** *81,* 109.
5. Dirac, P. A. M. *Proc. R. Soc. London, Ser. A* **1927,** *114,* 710.
6. Raman, C. V. *Nature* **1928,** *121,* 501. *Ind. J. Phys.* **1928,** *2,* 387.
7. (a) Rocard, Y. *Comptes Rendus Acad. Sci.* **1928,** *186,* 1107–1109. (b) Cabannes, J. *Comptes Rendus Acad. Sci.* **1928,** *186,* 1201–1202.
8. Landsberg, G.; Mandelstram, L. *Naturwissenschaften* **1928,** *16,* 557, 772.
9. Placzek, G. Rayleigh-Streuung und Raman-Effekt. In *Handbuch der Radiologie;* Marx, E., Ed.; Academische-Verlag: Leipzig, Germany, 1934; Vol. VI.2, p 205.
10. Daure, M.; Cabannes, M. *Rev. Optique, Theorique Instrum.* **1928,** *7,* 450–456.
11. Zworykin, V. K.; Rajchman, J. A. *Proc. Inst. Radio Eng.* **1939,** *27,* 558–566.
12. Morton, G. A. *Appl. Opt.* **1968,** *7,* 1–20.
13. Townes, C. H. In *Advances in Quantum Electronics;* Singer, J. R., Ed.; Columbia University Press: New York, 1961; pp 3–11.
14. Weber, A.; Porto, S. P. S. *J. Opt. Soc. Am.* **1965,** *55* (8), 1033–1034.
15. Czerny, M.; Turner, A. F. *Z. Phyzik.* **1930,** *61,* 792.
16. Sergent-Rozey, M. *Rev. Optique* **1965,** *44,* 193–203.
17. Arie, G.; Lescouarch, J. Cl.; Demol, R. *Nouv. Rev. Optique Appliquee* **1972,** *3* (5), 281–284.
18. Shafer, A. B.; Megill, L. R.; Droppleman, L. *J. Opt. Soc. Am.* **1964,** *54,* 879–887.
19. Reader, J. *J. Opt. Soc. Am.* **1969**, *59* (9), 1189–1196.
20. Grayzel, R.; Leclercq, M.; Adar, F.; Hutt, M.; Diem, M. An Automated Micro–Macro Raman Spectrograph System with Multichannel and Single-Channel Detectors in a New Molecular/Crystalline Microprobe. In *Microbeam Analysis;* Armstrong, J. T., Ed.; San Francisco Press: San Francisco, 1985; pp 19–25.
21. Leclercq, M. Etude de Premonochromateurs Soustractifs et de Spectrometers Raman a Reseaux Holographiques Concaves. Ph.D. Thesis, L'Universite des Sciences et Techniques de Lille, Lille, France, 1975.
22. Leclercq, M.; Walart, F. *J. Raman Spectrosc*. **1973,** *1,* 578–593.
23. Katzenberger, J. M.; Adar, F.; Lerner, J. M. An Improved Algorithm for Linearizing in Wavelength or Wavenumber Spectral Data Acquired with a Diode Array. In *Microbeam Analysis;* Geiss, R. H., Ed.; San Francisco Press: San Francisco, 1987; p 165.
24. Delhaye, M.; Migeon, M. *C. R. Acad. Sc. Paris* **1966,** *262,* 702–705.
25. Delhaye, M.; Migeon, M. *C. R. Acad. Sc. Paris* **1966,** *262,* 1513–1516.
26. Hirschfeld, T. *J. Opt. Soc. Am.* **1973,** *63,* 476.
27. Rosasco, G. J.; Etz, E. Investigation of the Raman Spectra of Individual Micron Sized Particles. In *Proceedings,* Fourth International Conference on Raman Spectroscopy, Brunswick, ME, Aug 25–29, 1974; Abstract 5.1.10.
28. Delhaye, M.; Dhamelincourt, P. Laser Raman Microprobe and Microscope. In *Proceedings,* Fourth International Conference on Raman Spectroscopy, Brunswick, ME, Aug 25–29, 1974; Abstract 5.B.
29. Delhaye, M.; Dhamelincourt, P. *J. Raman Spectrosc*. **1975,** *3,* 33–43.
30. Dhamelincourt, P. Instrumentation and Recent Applications in Micro Raman Spectroscopy. In *Microbeam Analysis;* Heinrich, K. F. J., Ed.; San Francisco Press: San Fancisco, 1982; pp 261–269.
31. Turrell, G.; Delhaye, M.; Dhamelincourt, P.; Characteristics of Raman Microscopy. In *Raman Microscopy;* Turrell, G., Corset, J., Eds.; Academic Press: London, 1996; Chapter 2.
32. Delhaye, M.; DaSilva, E.; Barbillat, J. European Patent No. 92400141.5, 1992.
33. Carrabba, M.; Spencer, K. M.; Rich, C.; Rauh, D. *Appl. Spectrosc*. **1990,** *44,* 1558–1561.
34. Tedesco, J. M.; Owen, H.; Pallister, D. M.; Morris, M. D.; *Anal. Chem*. **1993,** *65,* 441A–449A.
35. Delcroix, J.-L. *Rev. Optique* **1948,** *27* (8–9), 493–509.
36. Harootunian, A.; Betzig, E.; Isaacson, M.; Lewis, A. *Appl. Phys. Lett.* **1986,** *70,* 1671.
37. Truchet, M.; Delhaye, M. Transmission Electron Microscope with Castaing's Electron X-ray and Laser Raman Probes for Simultaneous Elemental and Molecular Analysis at Submicrometric Scale. In *Microbeam Analysis;* Geiss, R. H., Ed.; San Francisco Press: San Francisco, 1987; pp 163–164.
38. Barbillat, J. Raman Imaging. In *Raman Microscopy;* Turrell, G., Corset, J., Eds.; Academic Press: London, 1996; Chapter 4.